Computer Assisted Methods in Engineering and Science
32(4): 333–354, 2025, https://doi.org/10.24423/cames.2025.1916

Characterization Method of the Damping in Harmonically Forced Two-State Piecewise Linear Elastic Structures

Bilal ALZUBAIDI*, Róbert K. NÉMETH

Budapest University of Technology and Economics, Faculty of Civil Engineering, Department of Structural Mechanics, Budapest, Hungary; e-mail: nemeth.robert@emk.bme.hu

* *Corresponding Author e-mail: bilal.alzubaidi@emk.bme.hu*

An equivalent viscous damping ratio is introduced to characterize the energy dissipation caused by the plastic impact in the periodic responses of piecewise linear elastic systems.

Keywords: equivalent viscous damping ratio, piecewise linear elastic structures, periodic response.

1. Introduction

While linear analysis has been the primary tool in structural engineering for a long time, the actual structural behavior is typically nonlinear. A special form of nonlinearity is piecewise linearity, where the stiffness of its structure depends on a current configuration, involving at least two states of different stiffness. Classic examples are structures with the opening and closing of cracks or gaps [1, 7, 16], and with suspension cables that can become slackened or tensioned [5], as long as the separated states remain elastic. As piecewise linear (PL) elasticity is a special form of nonlinearity, the vibration characteristics of PL elastic structures under harmonic forcing are nonlinear, typically ending in chaotic behavior [8, 13]. Still, the periodic responses of nonlinear systems to harmonic forcing play a crucial role in the analysis of nonlinear vibrations as they serve as the starting points for further analyses depending on the stability of said responses. Examples include [14, 16].

In [1] the authors formulated an effective method for finding the periodic steady-state responses of two-state PL elastic structures, where the structure switches between the two states in both directions exactly once during a period

of forcing. The multi-degree-of-freedom (MDOF) model in the derived method experiences a plastic impact during one of the switches, which results in repetitive energy loss. Thus, even though the model is undamped, the plastic impact introduces an energy-dissipating effect balancing the energy added by the forcing to the system in the periodic motion. A more detailed analysis with finer discretization reveals that this impact-caused loss becomes negligible as the continuum limit is approached [17, 18]. The assumption of a perfectly plastic impact, where coefficient of restitution equals 0, is only an idealization for the true behavior of impacting structures. Actually, the material at the impact surface experiences partial plastification, similar to what is observed in reinforced concrete earthquake-resistant self-centering rocking structures [2]. Assuming one impact per period of forcing naturally creates a two-state system, while the method presented in [1] can be enhanced to include more impacts per period.

In this paper, the aim is to characterize this damping using a substitute viscous damping ratio. For this purpose, a formula will be derived for the calculation of a structural damping ratio that results in the same energy dissipation during a period of steady-state response as the energy loss occurring at the plastic impact. Viscous damping is specifically chosen as a substitute because in the structural engineering practice it is used as a single parameter, i.e., structural damping ratio.

There are various examples in structural engineering where viscous damping is used as a substitute for other forms of energy dissipative effects. Plastic deformation (yielding), resulting in hysteretic behavior of the steel materials during an earthquake, is one such example of that. In an early approximation, linearization was suggested by [3], and aimed to create an equivalent single-degree-of-freedom (SDOF) system with harmonic excitation. The stiffness degradation of the material was added to this in [4], while the direct displacement-based design (DDBD) method was suggested in [6] to handle general forcing instead of harmonic one. One of the steps in the earthquake analysis of structures using the DDBD method is to calculate an equivalent viscous damping ratio (EVDR) to account for the damping caused by hysteretic behavior. In a later study [10], a comparison between different EVDR models was done, and a new optimized value was proposed through nonlinear regression analysis. Beyond the nonlinearity caused by yielding, further possible nonlinearities include friction [14] or the combination of impact and friction [9]. PL elasticity is the simplest form of nonlinearity in the sense that each state can be treated as a linear system.

In PL elastic continuum structures, only an infinitesimal mass stops at the impact; thus, accounting for energy loss requires the inclusion of a proper constitutive law. Related to this, one can find recent studies that consider the nonsmooth modal analysis of bars in tension and compression, as in [11, 12, 18]. These studies found periodic motions for a presumed period in each state of

vibration. In continuum structures, the numerical model itself can be a source of energy loss: truncated modal analysis neglects higher vibration modes and their energies. The characterization of that energy loss under free vibration was studied in [15].

In this study, the classical structural engineering approach with a viscous damping ratio is applied to characterize the energy dissipation caused by plastic impact during the dynamic event of PL elastic structures. The novelty here is that the energy loss due to a single plastic impact is substituted with an EVDR by dispersing the instantaneous energy loss over a whole vibration period, a linearization concept that is of relevance to approaches used in structural engineering applications. The first aspect of the linearization performed is to treat this nonlinear system as two separate linear systems and utilize modal analysis to find its periodic motions. The second aspect of the linearization is to distribute the linear damping force over the whole period of vibration, where both linear systems undergo the same harmonic forcing as the PL elastic system. A formula for the EVDR is provided for forced MDOF PL elastic systems and calculated for each of the periodic solutions. Knowing this formula, the effect of loading position on the EVDR at different sections of the periodic paths is studied. Finally, the effect of the selected discrete model on its EVDR is shown.

The outline of the paper is as follows: in Sec. 2, the mechanical model of the PL elastic systems is revised with the previously introduced method of calculating the nonlinear periodic responses of such systems. In Sec. 3, the theoretical background for computing the internal energies of PL elastic systems is summarized, and the concept of linearization is presented to obtain an analytical formula for the EVDR. In Sec. 4, the application of our derived formula is demonstrated, where a discretized model of a simple system, a bar in tension and compression, is presented. Periodic paths and vibrations are calculated, and then the EVDR is calculated. The effects of vibration mode, forcing position, and discretization on the evaluated damping ratio are analyzed. Finally, the results are summarized in Sec. 5.

2. The PL elastic system with two states

2.1. The analyzed PL elastic mechanical models

In the practical structural engineering world, piecewise linearity can appear in various forms. Opening and closing of cracks in reinforced concrete or masonry structures are typical examples of that, where closing a crack yields a higher stiffness in the structure than in the structure with an open crack. Gaps in the initial stage of construction have the same mechanical role depending on whether they are open or closed. Slacking of suspension cables has a similar effect as well:

while a cable cannot resist compressive forces, its contribution to the structure's stiffness is absent in the slacked state.

In this research, the analysis is restricted to two-state systems only with N masses, and the impact of one mass during vibration is assumed to be perfectly plastic. State I corresponds to the configuration with the last mass in contact (constrained), hence the number of active DOFs in this state is $N^I = N - 1$, whereas state II has all masses free, giving $N^{II} = N$ DOFs. The switch from state I to state II occurs when the contact force drops to zero (gap opens), and the switch from state II to I occurs when the gap closes and the mass impacts, at which point its velocity is set to zero (plastic impact). Furthermore, there is no prestress in the current model: the unloaded state of the system can be considered to belong to both of the states, i.e., the impacting surfaces are in contact with zero force.

With harmonic forcing, the matrix differential equation of motion in state α, where α can be I or II, is:

$$\mathbf{M}^\alpha \ddot{\mathbf{x}}^\alpha(t) + \mathbf{K}^\alpha \mathbf{x}^\alpha(t) = \mathbf{q}_0^\alpha \cos(\omega t - \phi). \tag{1}$$

In the above equations, $\mathbf{M}^\alpha$ and $\mathbf{K}^\alpha$ are the mass and stiffness matrices in the α state, $\mathbf{x}^\alpha(t)$, $\ddot{\mathbf{x}}^\alpha(t)$ and $\mathbf{q}_0^\alpha$ are the vectors of displacements, accelerations and forcing amplitudes, respectively, which belong to state α and have a size of N^α-by-1. The symbols ω and ϕ are the forcing frequency and its phase angle, respectively. In the current analysis, harmonic forcing is applied to assume a worst-case scenario for the system, and the excitation is allowed on the masses moving in both states, i.e., any forcing on the impacting mass is excluded.

2.2. Modal analysis of the PL elastic model

The solutions of the differential equations of motion are performed using modal analysis. The displacement of the structure in state α is written as a linear combination of the eigenvectors:

$$\mathbf{x}^\alpha = \mathbf{V}^\alpha \boldsymbol{\eta}^\alpha, \tag{2}$$

where $\mathbf{V}^\alpha$ is the N^α-by-N^α modal matrix of the mass normalized eigenvectors, α can be I or II, and $\boldsymbol{\eta}^\alpha$ is the N^α-by-1 vector of modal coordinates. In the modal space, the modal force is represented by the projection of the forcing vector over the mode shapes for each state:

$$\mathbf{f}_0^\alpha = \mathbf{V}^{\alpha\top} \mathbf{q}_0^\alpha. \tag{3}$$

At certain time instants during the vibration, the system changes its state depending on the conditions around the boundary and its interaction with the

contact surface. The unilateral contact can be formulated as the one-dimensional form of the Signorini conditions [17].

The system remains in state I as long as there is a compressive reaction force at the contact surface, and the sign of the reaction force can be obtained from the spring force in the spring connecting the mass in contact, which is only affected by the displacement of them. Thus, the condition on the reaction force can be represented by the following inequality:

$$\mathbf{h}^{I\top}\mathbf{x}^{I} \geq 0. \tag{4}$$

The vector $\mathbf{h}^{I}$ is the N^{I}-th unit vector, ensuring that the force in the last spring will be in compression in order to maintain a positive reaction force. Similarly, the system remains in state II as long as there is a gap between the contact surfaces. Generally, this can be represented by the following inequality:

$$\mathbf{h}^{II\top}\mathbf{x}^{II} \geq 0. \tag{5}$$

The vector $\mathbf{h}^{II}$ is the opposite of the N^{II}-th unit vector, making sure that the last DOF does not penetrate the wall. Here, we note that Eqs. (4) and (5) are not used to decide the current state of motion, but only to check if the system remains in the currently assumed state. Specifically, in state II, the constraint in Eq. (5) must be true, whereas Eq. (4) is irrelevant until the switch from state II to I, the $\mathbf{h}^{I\top}\mathbf{x}^{I}$ product, even if only formally, could be negative, as well.

The system is assumed to switch between states at the time instant $t = t_s$. The system switches from state I to state II at $t_s = T^{I}$. The transformation of the displacements and velocities at this switch can be written as:

$$\mathbf{x}^{I} = \mathbf{X}^{I}\mathbf{x}^{II}, \qquad \mathbf{v}^{I} = \mathbf{Y}^{I}\mathbf{v}^{II}, \tag{6}$$

where $\mathbf{X}^{I}$ and $\mathbf{Y}^{I}$ matrices represent the relationship between the displacements and velocities of the DOFs in the two states. Substituting Eq. (2) into Eq. (6) yields:

$$\mathbf{V}^{I}\boldsymbol{\eta}^{I}(t_s) = \mathbf{Y}\mathbf{V}^{II}\boldsymbol{\eta}^{II}(t_s), \qquad \mathbf{V}^{I}\dot{\boldsymbol{\eta}}^{I}(t_s) = \mathbf{Y}\mathbf{V}^{II}\dot{\boldsymbol{\eta}}^{II}(t_s). \tag{7}$$

Using the normalization and orthogonality of the eigenvectors, multiplication of Eq. (7) from the left by $\mathbf{V}^{I\top}\mathbf{M}^{I}$ yields the switching of the modal coordinates and velocities from state II to state I:

$$\boldsymbol{\eta}^{I}(t_s) = \mathbf{V}^{I\top}\mathbf{M}^{I}\mathbf{Y}\mathbf{V}^{II}\boldsymbol{\eta}^{II}(t_s), \qquad \dot{\boldsymbol{\eta}}^{I}(t_s) = \mathbf{V}^{I\top}\mathbf{M}^{I}\mathbf{Y}\mathbf{V}^{II}\dot{\boldsymbol{\eta}}^{II}(t_s). \tag{8}$$

For brevity, the following matrices are introduced:

$$\mathbf{P}^{II} = \mathbf{V}^{I\top}\mathbf{M}^{I}\mathbf{X}^{I}\mathbf{V}^{II}, \qquad \mathbf{Q}^{II} = \mathbf{V}^{I\top}\mathbf{M}^{I}\mathbf{Y}^{I}\mathbf{V}^{II}, \tag{9}$$

which represent the projection from one modal space to another. Therefore, the switch of the modal displacements and velocities from state *II* to state *I* can be written in matrix form as:

$$\boldsymbol{\eta}^{I}(t_s) = \mathbf{P}^{II}\boldsymbol{\eta}^{II}(t_s), \qquad \dot{\boldsymbol{\eta}}^{I}(t_s) = \mathbf{Q}^{II}\dot{\boldsymbol{\eta}}^{II}(t_s). \tag{10}$$

Conversely, to describe the switch from state *I* to state *II*, a similar procedure can be followed, except that the *I* and *II* indices of the vectors and matrices must be exchanged.

2.3. Periodic modes of the PL elastic system with two states

The method proposed for the calculation of periodic vibrations in [1] is briefly explained in this section. The periodic responses searched for with this method are those, in which during one period of forcing, $T = 2\pi/\omega$, and for a certain forcing phase ϕ, the system first spends a yet unspecified T^I time in state *I*, performs a switch to state *II*, spends the $T^{II} = T - T^I$ time in state *II*, and then performs a switch back to state *I*.

The natural approach to find such responses includes finding the initial (modal) displacements and velocities, the forcing period T, and the forcing phase ϕ. Such a relatively large number of parameters creates a high-dimensional parameter space, where the scanning involves such a large computational demand that only path-following methods can be used efficiently. Furthermore, finding a good starting point for path-following must be done in the same space. Another difficulty with this approach is predicting sufficiently accurate initial conditions at the beginning to find one or more periodic paths.

The proposed method is different in the following way:

- First, the main parameters are T^I, T^{II} and ϕ, thus the period of vibration is consequently $T = T^I + T^{II}$, and ϕ is the phase of the forcing such that at $t = 0$, the system enters state *I*.
- Second, a linear system of equations is constructed to obtain the initial conditions that generate a periodic response for any T^I, T^{II} and ϕ triplet with the assumption that the system remains in its designated state. In addition to the harmonic behavior of the vibration modes, the switching formulae of Eq. (10) (and its *I*–*II* exchanged version) can be used.
- Third, the switch should happen at the desired times. This will lead to formulating two error functions that give the solutions in the scanned 3D parameter space on 1D manifolds.
- Finally, a time-history analysis is performed to filter out solutions from the 1D manifold where no premature switches occur.

The relatively low number of assumed parameters T^I, T^{II} and ϕ serves as a general representation space that can be scanned with reasonable computational effort. For computational details of the above steps, the reader is referred to [1].

3. Calculation of the EVDR

3.1. Kinetic energy of the PL elastic system with two states during one period

At the time instant $t = T^I + T^{II}$, the system experiences a plastic impact at the contact surface, causing one mass to stop and the system to switch from state *II* back to state *I*. Since the kinetic energy is directly related to the velocity, a part of it is associated with the motion of the stopping DOF, is lost in this incident, while the potential energy passes to the next period of vibration without any loss.

The kinetic energy of the system in state α is calculated from the velocities of the DOFs or the modes as:

$$\mathcal{E}_K^\alpha(t) = \frac{1}{2}\dot{\mathbf{x}}^{\alpha\top}(t)\mathbf{M}^\alpha\dot{\mathbf{x}}^\alpha(t) = \frac{1}{2}\dot{\boldsymbol{\eta}}^{\alpha\top}(t)\mathbf{V}^{\alpha\top}\mathbf{M}^\alpha\mathbf{V}^\alpha\dot{\boldsymbol{\eta}}^\alpha(t). \tag{11}$$

As a result of the mass normalization of the mode shapes, the matrix triple product $\mathbf{V}^{\alpha\top}\mathbf{M}^\alpha\mathbf{V}^\alpha$ forms identity matrices; therefore, we can get to the kinetic energy as the sum of the modal kinetic energies in state α:

$$\mathcal{E}_K^\alpha(t) = \frac{1}{2}\sum_{j=1}^{N^\alpha}\dot{\eta}_j^{\alpha 2}(t). \tag{12}$$

Similarly, the internal potential energy (originating from the stiffness matrix) will be:

$$\mathcal{E}_P^\alpha(t) = \frac{1}{2}\sum_{j=1}^{N^\alpha}{\omega_{0j}^\alpha}^2\eta_j^{\alpha 2}(t). \tag{13}$$

The plastic impact at $t = T$ causes an energy loss, which can be calculated from the change in kinetic energy:

$$\Delta_{\mathrm{PL}} = \mathcal{E}_K^{II}(T) - \mathcal{E}_K^I(T) = \frac{1}{2}\sum_{j=1}^{N^{II}}\dot{\eta}_j^{II2}(T) - \frac{1}{2}\sum_{j=1}^{N^I}\dot{\eta}_j^{I2}(0). \tag{14}$$

(Note: due to the periodicity, $\dot{\eta}_j^\alpha(t) = \dot{\eta}_j^\alpha(t+T)$, so the subtracted second sum is the same as at $t = T$). In the next subsection, a method for how this energy loss can be distributed over all modes of the periodic vibration using a viscous damping coefficient is proposed.

3.2. Equivalent viscous damping ratio for the forced PL elastic system with two states

As mentioned earlier, viscous damping is widely used in civil engineering practice to account for energy losses during nonlinear responses in dynamically loaded structures. In our nonlinear system, the linear combination of the linear vibration modes in Eq. (2) is utilized to find the periodic responses. We can also employ the piecewise linearity to define equivalent linear counterparts by assuming that both systems undergo harmonic forcing with the same $T = T^I + T^{II}$ period and phase angle ϕ as the solution triplets for the PL elastic system. Apart from the near-to-resonant cases, a small viscous damping ratio slightly modifies the undamped response (amplitude and phase). Using this, the velocities of the damped system are approximated with the velocities of the undamped response. The energy loss is then calculated piecewise as that of a linear system with a constant viscous damping ratio in both states for each mode. In this way, linearity can still be kept in the sense that we can disperse the damping force along the whole period using simple mechanics and find a single VDR as our ultimate goal.

During the modal analysis of MDOF systems, each mode behaves as an SDOF oscillator. So, a formula for estimating the energy loss of an SDOF system with a unit mass and an ω_0 natural circular frequency is needed. The viscous damping force is linearly proportional to the velocity of the system, which can be expressed as:

$$\dot{\eta}(t) = \psi_1 + \psi_2 + \psi_3, \tag{15}$$

where:

$$\psi_1 = -\omega_0 a \sin(\omega_0 t), \qquad \psi_2 = \omega_0 b \cos(\omega_0 t), \tag{16}$$

$$\psi_3 = \frac{q_0}{\omega_0^2} \frac{1}{1 - \frac{\omega^2}{\omega_0^2}} \omega \left(\sin\phi \cos(\omega t) - \cos\phi \sin(\omega t)\right). \tag{17}$$

Here, ω is the forcing frequency and ω_0 is the natural circular frequency of the SDOF. The term ψ_3 is the particular solution of the harmonically forced vibration, while $\psi_1 + \psi_2$ is the free vibrational part. Thus, a and b are the constants used to fulfill the initial conditions, and their formulae are given in Appendix 1. (Note: for the modal analysis of the PL system, the modal initial conditions will originate from the switch to a current state.) The amplitude of the particular response consists of the product of a static displacement, a coefficient of resonance and the time-dependent part.

Assuming that ξ is the damping ratio, the damping force in the current SDOF system is $2\omega_0\xi\dot{\eta}(t)$. Its energy dissipation during a time interval T^* is written as:

$$E_D = \int_{T^*} 2\omega_0\xi\,\dot{\eta}^2(t)dt. \tag{18}$$

Substituting Eqs. (16) and (17) into Eq. (18) and writing it in a compact form yields:

$$E_D = 2\omega_0\xi\Psi, \tag{19}$$

where

$$\Psi = \int_{T^*} \dot{\eta}(t)^2 dt = \int_{T^*} \Big[\psi_1^2 + \psi_2^2 + \psi_3^2 + 2\left(\psi_1\psi_2 + \psi_2\psi_3 + \psi_3\psi_1\right)\Big] dt. \tag{20}$$

The analytical results of the integration of the ψ^2 functions and their products are detailed in Appendix 2.

In a PL MDOF system, for each mode, Eqs. (15)–(20) must be modified according to the current α value and the j index of the mode. In state I, the T^* integration domain will be between 0 and T^I. In state II, the T^* integration domain will be between T^I and T. Finally, for the MDOF PL elastic system, the summation of the modes is taken for the Ψ^α functions in each state as:

$$\Delta_d = 2\xi\left(\sum_{j=1}^{N^I}\Psi_j^I\omega_{0j}^I + \sum_{j=1}^{N^{II}}\Psi_j^{II}\omega_{0j}^{II}\right). \tag{21}$$

The equivalent damping ratio is obtained from Eqs. (14) and (21), i.e., solving $\Delta_d = \Delta_{\mathrm{PL}}$ for ξ yields:

$$\xi_{eq} = \frac{\Delta_{\mathrm{PL}}}{2\left[\sum\limits_{j=1}^{N^I}\Psi_j^I\omega_{0j}^I + \sum\limits_{j=1}^{N^{II}}\Psi_j^{II}\omega_{0j}^{II}\right]}. \tag{22}$$

Once the periodic paths of the PL elastic structure are available, this formula is used to calculate ξ_{eq} for these paths.

This approach assumes that ξ_{eq} is small, so that the difference between the undamped and damped motions is negligible for the first order. In our results, ξ_{eq} indeed comes out on the order of a few percent, validating this assumption a posteriori. For larger damping values, a more involved iterative approach might be required to update the velocity profile.

For the practical application of Eq. (22), the following approach is recommended. With certain simple load positions, the periodic paths of the structure can be obtained. Then, using Eq. (22), the corresponding equivalent viscous damping ratio can be calculated for each mode. For the analysis of the PL elastic structure with a general loading, the linear elastic model can be used with ξ_{eq} chosen from the obtained range of the periodic results. In the following examples, these steps mentioned above are applied to the mass-spring model introduced in Fig. 1.

4. Examples: Forced discrete model of a PL elastic bar in tension and compression

In this section, the application of the derived formula in Eq. (22) is demonstrated through a simple example. The applied structure is a mass-spring model with N degrees of freedom. All DOFs have the same mass of m, and they are serially connected by the springs of the same stiffness k. One end of the model is constrained by a rigid wall, while the other end has a unilateral contact, see Fig. 1a. This unilateral contact divides the motion into two linear states of stiffness. The first state is the sticking state, herein after called *state I*, where the last mass is in contact with the wall, so the number of masses contributing to the equation of motion is $N^I = N - 1$ (see Fig. 1b). The second state is the free-flight state, herein after called *state II*, where the last mass is free from contact, so the number of masses is $N^{II} = N$ (see Fig. 1c).

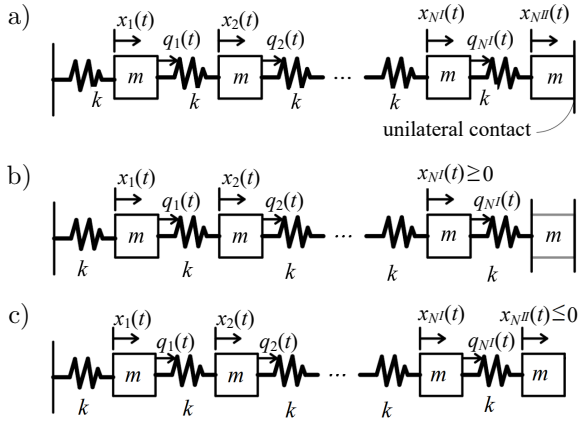

FIG. 1. PL elastic system: a) system at equilibrium, b) state *I*, and c) state *II*.

In our examples, the $\mathbf{M}^I$ and $\mathbf{K}^I$ matrices are the mass and stiffness matrices, respectively, for state I and have a size of N^I-by-N^I:

$$\mathbf{M}^I = \begin{bmatrix} m & & & \\ & m & & \\ & & \ddots & \\ & & & m \end{bmatrix}, \qquad \mathbf{K}^I = \begin{bmatrix} 2k & -k & & \\ -k & 2k & \ddots & \\ & \ddots & \ddots & -k \\ & & -k & 2k \end{bmatrix}. \tag{23}$$

The matrices $\mathbf{M}^{II}$ and $\mathbf{K}^{II}$ are the mass and stiffness matrices, respectively, for state *II* and have a size of N^{II}-by-N^{II}:

$$\mathbf{M}^{II} = \begin{bmatrix} m & & & & \\ & m & & & \\ & & \ddots & & \\ & & & m & \\ & & & & m \end{bmatrix}, \qquad \mathbf{K}^{II} = \begin{bmatrix} 2k & -k & & & \\ -k & 2k & \ddots & & \\ & \ddots & \ddots & -k & \\ & & -k & 2k & -k \\ & & & -k & k \end{bmatrix}. \tag{24}$$

In state *I*, the reaction force R acting on the last mass (in contact with the wall) cannot be a tension; in state *II*, the last mass cannot penetrate the wall, i.e., its displacement cannot be positive. Furthermore, at least one of these two variables must be zero. These constraints result in two inequalities and one equation:

$$R \leq 0, \qquad x_{N^{II}} \leq 0, \qquad R x_{N^{II}} = 0. \tag{25}$$

However, in the proposed form of analysis, it is sufficient to maintain one inequality at a time, as the closed or open state of the gap is secured in the numerical models of states *I* and *II*. Thus, the applied conditions will represent the gap opening: switching from state *I* to *II*, where the $\mathbf{h}^I$ vector of Eq. (4) is the N^I-th unit vector; or the gap closing: switching from state *II* to *I*, where the vector $\mathbf{h}^{II}$ in Eq. (5) is the *opposite* of the N^{II}-th unit vector.

In the numerical examples, the values $m = 1$ and $k = 1$ will be used. Changing these parameters would affect the time scale, but the ratios of the numerical values in the found solutions remain the same.

4.1. Periodic vibrations, energy loss and equivalent viscous damping ratios

For our first example, $N = 5$ is chosen, and the harmonic forcing of unit amplitude acts on the first DOF (i.e., $q_{01}^{\alpha} = 1$), while the other DOFs are not excited. (Note: scaling the amplitude of the forcing would scale the response at the same rate, but the time remains unaffected due to the PL elastic nature of the structure.)

The periodic modes were calculated by scanning the global representation space (GRS) of (T^I, T^{II}, ϕ) according to the method described in Subsec. 2.3. The time period in each state ranged from zero to half of the fundamental period of the relevant state, and the phase angle (ϕ) varied from π to 2π. The 3D GRS was discretized on a $200 \times 200 \times 50$ grid. After filtering out the solution candidates that undergo premature switches, two separate curves of periodic modes, shown in Figs. 2a and 2b, (an axonometric and a planar view, respectively) were obtained. Along these paths lie those T^I, T^{II} and ϕ triplets that lead to vibrations that fulfill the periodicity and switching conditions of the method. The isolated positioning of these two curves illustrates the robustness of the proposed scanning method. The first segment is near the base period of state I (10.166 in this example), while the second segment is near half of the base period of state II (half of 22.075 in this example). A sample point is taken randomly from each path (shown as red and green dots in Fig. 2b) to demonstrate those nonlinear periodic vibrations.

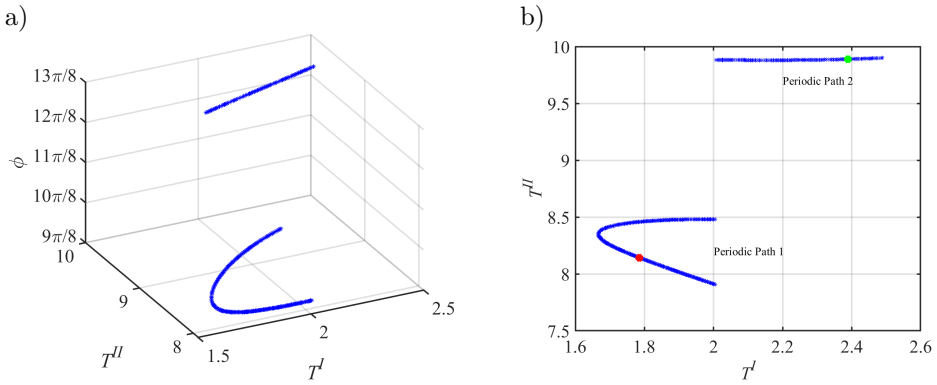

FIG. 2. Solution points of a system with $N = 5$ and the first mass forced: a) in the three-dimensional parameter space, b) in the $T^I - T^{II}$ plane.

The responses of each DOF at the sample points are shown in Fig. 3, plotted over approximately two of their respective periods (the starting points of the periods are marked by vertical, red, dashed lines). Figure 3a shows the diagrams of the red-marked point in Fig. 2b, with a period $T = 9.9273$, while Fig. 3b shows the diagrams of the green-marked point, with a period $T = 12.277$. The I-to-II switch can be observed, where the fifth DOF starts moving at $t = T^I$.

Once the periodic modes are available, the kinetic energy, internal potential energy and their sum during the vibration can be evaluated. These energies were calculated for the sample points marked with the green and red dots in Fig. 2b using Eqs. (12) and (13), and are shown in Fig. 4.

Figure 4a shows the time-histories of the energies for the solution marked with the red dot. The total energy is not constant due to the forcing. The system

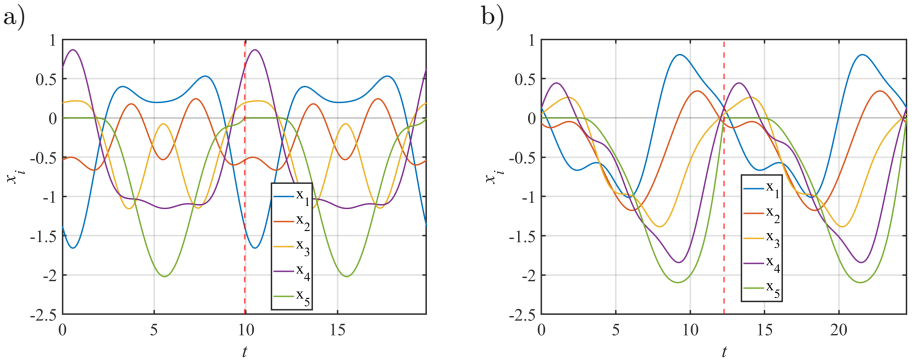

FIG. 3. Nonlinear periodic responses of the system at coordinates:
a) $T^I = 1.7748$, $T^{II} = 8.1525$, $\phi = 3.5495$ (red dot, vertical dashed line at $T = 9.9273$);
b) $T^I = 2.3876$, $T^{II} = 9.8894$, $\phi = 4.8050$ (green dot, vertical dashed line at $T = 12.277$).

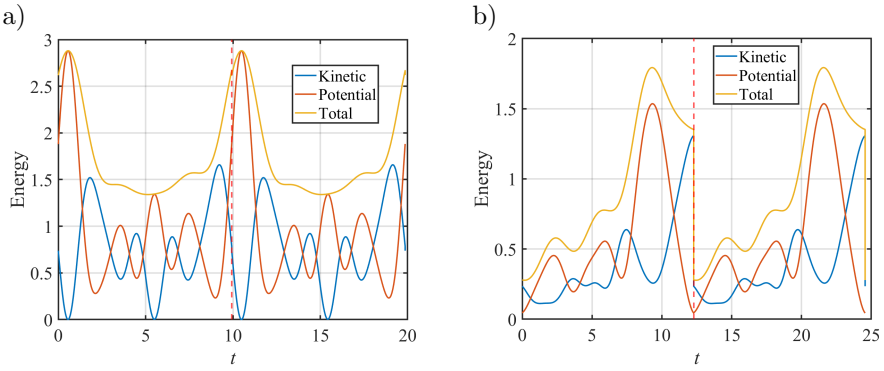

FIG. 4. Mechanical energy at the sample point at: a) red dot in Fig. 2b (vertical dashed line at $T = 9.9273$), b) green dot in Fig. 2b (vertical dashed line at $T = 12.277$).

switches from state *II* to state *I* at the period's end (marked with the dashed line), where a drop in kinetic energy occurs due to the sudden stoppage of x_5. (In Fig. 3a, its slope becomes zero at the start of the next period.) Please note that the internal potential energy does not undergo such sudden changes. Similarly, Fig. 4b shows the time histories of the energies for the solution marked with the green dot. In this case, energy has a higher share of kinetic energy, and the last mass contributes more, so a drop in energy is of higher rate.

Next, the energy loss was calculated for every solution point in Fig. 2. In Fig. 5a, the dissipated energies of the PL elastic system are shown as a function of the period of forcing T and the phase of the forcing ϕ by the blue curves. The nature of the vibration modes is similar along the isolated branches of the solution points, and the dissipated energy is longer in the cases where the kinetic energy of the stopping DOF is higher before the impact. However, the conversion of this energy loss to a damping ratio involves the amplitude of the response as well.

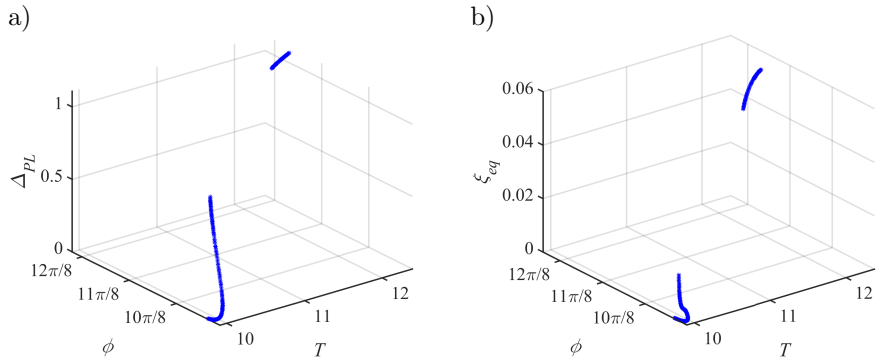

FIG. 5. a) Energy loss of the PL system Δ_{PL} as a function of the total period of forcing and phase angle; b) equivalent viscous damping ratio as a function of T and ϕ.

Finally, Fig. 5b shows the relationship between the forcing parameters T and ϕ for both periodic paths and the obtained ξ_{eq} (see Eq. (22)). The magnitudes are small and a maximum does not exceed the 5–10% value typically assumed in the civil engineering practice for the structural damping ratio. For better understanding and to distinguish between the different orders of magnitude of the segments, the damping ratio values are presented separately for the first and the second path in Figs. 6a and 6b.

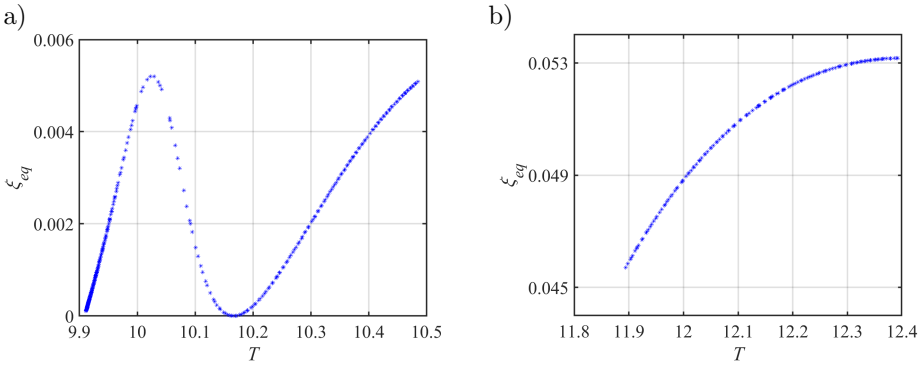

FIG. 6. Equivalent viscous damping ratio for: a) periodic path 1, b) periodic path 2.

Along the first path, not only are the energy losses smaller, but they are also associated with a lower impact velocity, so their equivalent viscous damping ratios (shown in Fig. 6a) are smaller than those of the second path (shown in Fig. 6b). The reason behind this phenomenon lies in the higher amplitudes of the vibration in the modes of the second path. This specifically yields a zero damping at the $T = 10.167$ case: this forcing is resonant in the state I, as the increasing amplitude in the first mode makes the lost energy negligible, while the amplitude of the stopping mass changes its sign.

What also can be concluded from Fig. 6b, for example, for the solution point at the green dot, is that if a linear system of $N = 5$ is assumed with a damping ratio around 0.052 under a forcing frequency of $\omega = 2\pi/12.277 = 0.512$, then the energy loss will be equal to the value of Δ_{PL} shown in the top right corner of Fig. 5a. This value can also be seen in Fig. 4b at the end of the period, which is around 1.05.

4.2. Effect of the loading position on ξ_{eq}

In this subsection, the effect of the position of the excitation force on the response and the equivalent viscous damping is analyzed on the same model used in the previous subsection with $N = 5$. A unit amplitude harmonic forcing is applied to the first, second, third and fourth DOFs, while the other DOFs are left unloaded, and the analyses are performed to find the periodic paths and the equivalent viscous damping ratios. It was found that scanning the GRS resulted in the same parameter triplets as those in Fig. 2, meaning that, in the GRS, the periodic solutions are independent of the loading position. The reason behind this similarity in the periodic paths of certain models is out of the scope of this paper, but likely can be explained in terms of traveling waves. While the GRS positions of the periodic modes coincide, different load cases result in different initial conditions and, thus, in different vibrations. Diagrams of Fig. 7 show the time histories of one single DOF under different load cases over one period. Figures 7a and 7b correspond to the periodic modes marked by the red and green dots, respectively. The second index in the diagrams corresponds to the DOF (in the diagrams of the 5th DOF the $0 - T^I$ segment remains zero). Finally, the colors represent the index of the forced DOF (the load case), a thick line indicates the response where the DOF itself is forced.

Next, the equivalent damping ratios are calculated for the found solution points. Figure 8a shows the resulting ξ_{eq} values for the first path of periodic modes. It can be seen that there are no significant differences in the values, which are already small, and the near-resonance phenomenon of vanishing ξ_{eq} persists. On the contrary, Fig. 8b shows the ξ_{eq} values for the periodic modes on the second path, which show a variation on a wider range. A maximum value occurs when the DOF near the middle of the structure is forced.

If the serially connected mass-spring model is considered as a discretized model of a bar in tension and compression, a general positioning of the load can be modeled as follows. Instead of using a single force on a DOF, the positioning between two adjacent DOFs can be shared. For example, a $q_{1,0} = 0.75$, $q_{0,2} = 0.25$ load combination means that the first quarter point of the segment between the first and second DOF is excited. (Here the reader is reminded that the actual amplitude of the forcing vanishes in the damping ratio.)

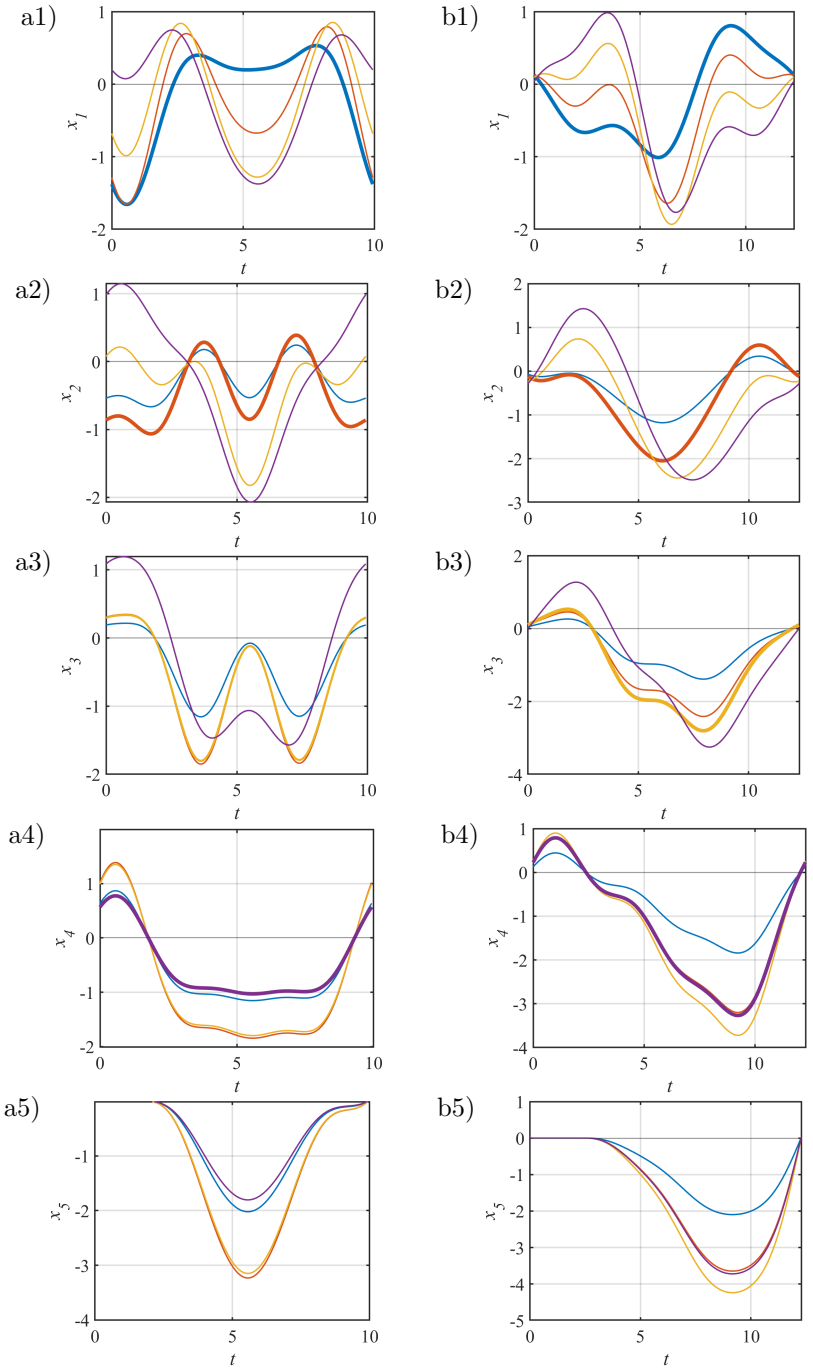

FIG. 7. Nonlinear periodic responses of the system for each mass for different loading scenarios at: a) periodic mode from path 1 (red dot) and b) periodic mode from path 2 (green dot). The color legend is as follows: only $q_{01}^{\alpha} = 1$ (blue), only $q_{02}^{\alpha} = 1$ (red), only $q_{03}^{\alpha} = 1$ (orange) and only $q_{04}^{\alpha} = 1$ (violet), with the forced mass with a thicker line width for each load case.

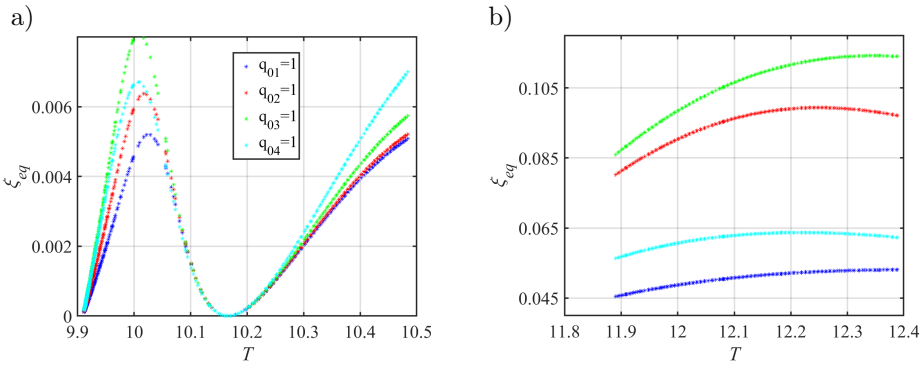

FIG. 8. Equivalent viscous damping ratio for different unit exciting force positions along: a) periodic path 1, b) periodic path 2.

The similarities of the solution paths in the GRS remain for the load combinations as well. Thus, the equivalent damping ratios of the same solution point can be compared in the GRS for different load positions. Figure 9c shows the obtained values, marked as red points, where a single node is excited (the red lines are polygonal approximations of the curves in Fig. 8b). From the diagram, it can be concluded that combining the simple load cases, where only one DOF is excited, does not result in an extreme increase in the damping ratio: in the excitation of one DOF, the maximum damping ratio is 0.1185, while in the combinations, the maximum is 0.121. Although linear interpolation may underestimate the values between the red points, the order of magnitude of the excess damping is way below the damping ratio of the cases with single-node excitation. So, in a practical application, it is a sufficient approximation to analyze the equivalent damping based on the excitation of certain DOFs, and there is no need to check all possible combinations.

4.3. Effect of the discretization on ξ_{eq}

In this subsection, the effect of discretization is analyzed. For the analysis of the discretized model of the bar in tension and compression, the mass m and the stiffness k should be tuned accordingly, depending on the number of DOFs. However, the scaling of the $\mathbf{M}$ and $\mathbf{K}$ matrices changes the time scale only; the damping ratio remains the same. So, the second periodic paths in the GRS of MDOF models with $N = 3$, $N = 4$, $N = 5$, and $N = 6$ are compared, i.e., the segments near half of the base period of state I. (In the analyzed models, these base periods are $T_0^3 = 14.12$, $T_0^4 = 18.09$, $T_0^5 = 22.07$, $T_0^6 = 26.06$, respectively.) Results are shown in Figs. 9a–d, where: the calculated viscous damping ratios are shown as a function of the period of the forcing and the (interpolated) position of the forcing. In the $N = 3$, $N = 5$, $N = 6$ models, the segments are

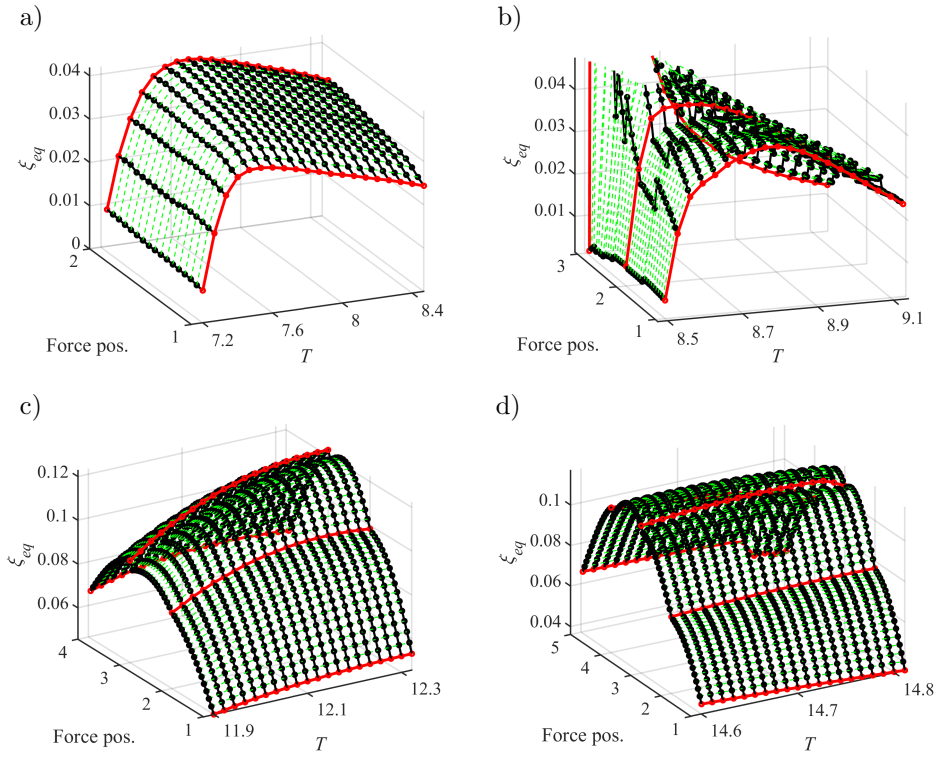

FIG. 9. Equivalent viscous damping ratio for different positions of the excitation force. Red dots represent modes where a single node is forced, and black dots represent modes where a combination is forced: a) $N = 3$, b) $N = 4$, c) $N = 5$, d) $N = 6$.

slightly above half of the said base period; in the $N = 4$ model, the segments are slightly below half of the base period.

Comparing the diagrams, it can be concluded that the extent of the possible periods decreases as a finer discretization (a higher number of DOFs) is applied. As a limit, it could shrink to a single point, meaning that the continuum bar would have a periodic response to a single harmonic frequency only.

In general, it is expected that the magnitude of the calculated damping ratio is decreasing, as the discretization becomes finer, as the share of the stopping mass and its kinetic energy is decreasing, in the continuum there would be no energy loss with the current assumption. This can be seen in the transition from $N = 5$ to $N = 6$, where the maximum decreases from 0.121 to 0.111. Further discretization would result in damping ratios below the value of 0.1. The reader is reminded here that structural engineering practice typically summarizes energy dissipation into one single structural damping ratio in the range of 0.05–0.1, which is the order of magnitude of the contribution from the impact of the PL system.

For cases with a low number of DOFs, due to the coarse discretization, the MDOF model can not follow the actual vibration accurately, so this effect cannot unfold in its full extent yet. This disturbance could lead to a low-amplitude vibration of the last mass, as in the case of $N = 3$ (Fig. 9a), where the obtained damping ratio (with a maximum of 0.0418) is lower than it would be with a finer discretization. The other directional disturbance, with a high-amplitude vibration of the last mass, occurs in the case of $N = 4$ (Fig. 9b) where the domain of the periodic path moves below half of the base period (in all the other cases it is above that), and forcing the third mass could lead to a vibration mode dominated by the motion (and stop) of the fourth mass. The resulting maximal damping ratio would be above 0.5, but this is rather a side effect of the insufficient discretization than a usable result. For this reason, the diagram Fig. 9b is limited at 0.045.

The following generalization of our findings is recommended. On a sufficiently fine discretized model, periodic paths can be computed with forcing a single DOF. Then, the calculation can be repeated in the obtained domains with other DOFs forced, and the damping ratios can be evaluated. From the resulting values, a maximum can be taken as an upper limit for a time-history analysis. It should be reminded that a plastic impact was assumed in our model; so, the obtained damping ratio can be considered an upper limit, as an inelastic impact results in a lower amount of dissipated energy.

5. Conclusion

In the present work, a formula for the equivalent viscous damping ratio was derived to characterize the energy dissipation caused by purely plastic impact in the forced PL elastic systems with two states. The formula is restricted to vibration modes where the response during a period of forcing consists of a given time spent in one state and the rest in the other state. This allows for the application of modal analysis for the calculation of the response and dissipated energy in a substitute system with an assumed viscous damping ratio. An example of a discretized bar in tension and compression was presented, and the values of ξ_{eq} were shown as a function of the forcing period. The results were presented for each periodic path. The ξ_{eq} values appeared to fall in the range of the damping ratio typical for engineering structures or were negligible under certain circumstances.

The effect of the loading position on the ξ_{eq} values was presented. The highest values appeared when the point load was applied near the middle of the structure. For example, for $N = 5$ and $N = 6$ cases, $\xi_{eq,\max} = 0.121$ and 0.111, respectively, and these maxima occurred between the 2nd and the 3rd DOFs for $N = 5$ case, and between the 3rd and the 4th for $N = 6$. In conclusion, for prac-

tical applications, it is sufficient to analyze the equivalent damping by forcing of certain DOFs, and therefore eliminating the need to check all possible combinations.

Appendix 1. Amplitude of free vibration terms

The free vibration amplitude mentioned in Eq. (16) is given by:

$$a^{\alpha} = \left[\eta^{\alpha}(t_s) - \eta^{\alpha}_{f0}\cos\phi\cos(\omega t_s) - \eta^{\alpha}_{f0}\sin\phi\sin(\omega t_s)\right]\cos(\omega^{\alpha}_0 t_s) - \left[\frac{\dot{\eta}^{\alpha}(t_s)}{\omega^{\alpha}_0} + \frac{\omega}{\omega^{\alpha}_0}\eta^{\alpha}_{f0}\cos\phi\sin(\omega t_s) - \eta^{\alpha}_{f0}\sin\phi\cos(\omega t_s)\right]\sin(\omega^{\alpha}_0 t_s), \tag{26}$$

$$b^{\alpha} = \left[\eta^{\alpha}(t_s) - \eta^{\alpha}_{f0}\cos\phi\cos(\omega t_s) - \eta^{\alpha}_{f0}\sin\phi\sin(\omega t_s)\right]\sin(\omega^{\alpha}_0 t_s) + \left[\frac{\dot{\eta}^{\alpha}(t_s)}{\omega^{\alpha}_0} + \frac{\omega}{\omega^{\alpha}_0}\eta^{\alpha}_{f0}\cos\phi\sin(\omega t_s) - \eta^{\alpha}_{f0}\sin\phi\cos(\omega t_s)\right]\cos(\omega^{\alpha}_0 t_s), \tag{27}$$

where $\eta^{\alpha}(t_s)$ and $\dot{\eta}^{\alpha}(t_s)$ are the initial conditions (displacement and velocity at $t = t_s$ is the time instance of the switch), and η^{α}_{f0} is the amplitude of the particular solution.

Appendix 2. Integrated terms of dissipated energy

The primitive functions of the quadratic and product terms in Eq. (20) are:

$$\int_{T^{\alpha}} \psi_1^{\alpha 2} = \omega_0^{\alpha 2} a^{\alpha 2}\left[\frac{t}{2} - \frac{\sin(2t\omega_0^{\alpha})}{4\omega_0^{\alpha}}\right]^{\alpha}, \tag{28}$$

$$\int_{T^{\alpha}} \psi_2^{\alpha 2} = \omega_0^{\alpha 2} b^{\alpha 2}\left[\frac{t}{2} + \frac{\sin(2t\omega_0^{\alpha})}{4\omega_0^{\alpha}}\right]^{\alpha}, \tag{29}$$

$$\int_{T^{\alpha}} \psi_3^{\alpha 2} = \omega^2 \frac{q_0^{\alpha 2}}{\omega_0^{\alpha 4}}\left(\frac{1}{1-\frac{\omega^2}{\omega_0^{\alpha 2}}}\right)^2\left[\cos^2\phi\left[\frac{t}{2} - \frac{\sin(2t\omega)}{4\omega}\right]^{\alpha} - \sin 2\phi\left[\frac{-\cos(2\omega t)}{4\omega}\right]^{\alpha} + \sin^2\phi\left[\frac{t}{2} + \frac{\sin(2t\omega)}{4\omega}\right]^{\alpha}\right], \tag{30}$$

$$\int_{T^{\alpha}} \psi_1^{\alpha}\psi_2^{\alpha} = -\omega_0^{\alpha 2} a^{\alpha} b^{\alpha}\left[\frac{-\cos(2\omega_0^{\alpha} t)}{4\omega_0^{\alpha}}\right]^{\alpha}, \tag{31}$$

$$\int_{T^\alpha} \psi_2^\alpha \psi_3^\alpha = -\, b^\alpha \omega \frac{q_0^\alpha}{\omega_0^\alpha} \frac{1}{1-\frac{\omega^2}{\omega_0^{\alpha 2}}} \cdot \left[\cos\phi \left[\frac{-\omega_0^\alpha \sin(\omega t)\sin(\omega_0^\alpha t) - \omega \cos(\omega t)\cos(\omega_0^\alpha t)}{\omega^2 - \omega_0^{\alpha 2}} \right]^\alpha - \sin\phi \left[\frac{\sin((\omega+\omega_0^\alpha)t)}{2(\omega+\omega_0^\alpha)} + \frac{\sin((\omega-\omega_0^\alpha)t)}{2(\omega-\omega_0^\alpha)} \right]^\alpha \right], \tag{32}$$

$$\int_{T^\alpha} \psi_3^\alpha \psi_1^\alpha = a^\alpha \omega \frac{q_0^\alpha}{\omega_0^\alpha} \frac{1}{1-\frac{\omega^2}{\omega_0^{\alpha 2}}} \cdot \left[\cos\phi \left[\frac{\omega_0^\alpha \sin(\omega t)\cos(\omega_0^\alpha t) - \omega \cos(\omega t)\sin(\omega_0^\alpha t)}{\omega^2 - \omega_0^{\alpha 2}} \right]^\alpha - \sin\phi \left[\frac{\cos((\omega-\omega_0^\alpha)t)}{2(\omega-\omega_0^\alpha)} - \frac{\cos((\omega+\omega_0^\alpha)t)}{2(\omega+\omega_0^\alpha)} \right]^\alpha \right]. \tag{33}$$

Acknowledgments

This work was supported by the Hungarian National Research, Development and Innovation Office (NKFIH): Grant No. 138615.

References

1. B. Alzubaidi, R.K. Németh, Modal analysis-based calculation of periodic nonlinear responses of harmonically forced piecewise linear elastic systems, *Journal of Sound and Vibration*, **549**: 117576, 2023, https://doi.org/10.1016/j.jsv.2023.117576.

2. M. Froozanfar, S. Moradi, R. Kianoush, M.S. Speicher, L. Di Sarno, Review of self-centering rocking systems for earthquake-resistant building structures: State of the art, *Journal of Building Engineering*, **84**: 108607, 2024, https://doi.org/10.1016/j.jobe.2024.108607.

3. L.S. Jacobsen, Steady forced vibration as influenced by damping: An approximate solution of the steady forced vibration of a system of one degree of freedom under the influence of various types of damping, *Transactions of the American Society of Mechanical Engineers*, **52**(2): 169–178, 1930, https://doi.org/10.1115/1.4057368.

4. P.C. Jennings, Equivalent viscous damping for yielding structures, *Journal of the Engineering Mechanics Division*, **94**(1): 103–116, 1968, https://doi.org/10.1061/JMCEA3.0000929.

5. A. Kocsis, R.K. Németh, B. Turmunkh, Dynamic analysis of a beam on block-and-tackle suspension system: A continuum approach, *Engineering Structures*, **101**: 412–426, 2015, https://doi.org/10.1016/j.engstruct.2015.07.022.

6. M.J. Kowalsky, M.J.N. Priestley, G.A. MacRae, Displacement-based design of RC bridge columns in seismic regions, *Earthquake Engineering & Structural Dynamics*, **24**(12): 1623–1643, 1995, https://doi.org/10.1002/eqe.4290241206.

7. G. Lengyel, R.K. Németh, Free vibration of a cracked, pre-stressed continuous rod, *Procedia Engineering*, **161**: 1656–1661, 2016, https://doi.org/10.1016/j.proeng.2016.08.641.

8. F. Li, X. Li, B. Li, H. Ma, B. Wen, Nonlinear dynamic modeling and vibration analysis of bearing system considering shaft current damage, *Mechanics Based Design of Structures and Machines*, **52**(2): 1190–1210, 2024, https://doi.org/10.1080/15397734.2022.2150639.

9. G. Li, S. Wu, H. Wang, W. Ding, Global dynamics of a non-smooth system with elastic and rigid impacts and dry friction, *Communications in Nonlinear Science and Numerical Simulation*, **95**: 105603, 2021, https://doi.org/10.1016/j.cnsns.2020.105603.

10. T. Liu, T. Zordan, Q. Zhang, B. Briseghella, Equivalent viscous damping of bilinear hysteretic oscillators, *Journal of Structural Engineering*, **141**(11): 06015002, 2015, https://doi.org/10.1061/(ASCE)ST.1943-541X.0001262.

11. T. Lu, M. Legrand, Nonsmooth modal analysis via the boundary element method for one-dimensional bar systems, *Nonlinear Dynamics*, **107**: 227–246, 2022, https://doi.org/10.1007/s11071-021-06994-z.

12. T. Lu, M. Legrand, Harmonic balance-based nonsmooth modal analysis of unilaterally constrained discrete systems, *Nonlinear Dynamics*, **112**: 1619–1640, 2024, https://doi.org/10.1007/s11071-023-09014-4.

13. G.W. Luo, X.H. Lv, Controlling bifurcation and chaos of a plastic impact oscillator, *Nonlinear Analysis: Real World Applications*, **10**(4): 2047–2061, 2009, https://doi.org/10.1016/j.nonrwa.2008.03.010.

14. G.W. Luo, X.H. Lv, L. Ma, Periodic-impact motions and bifurcations in dynamics of a plastic impact oscillator with a frictional slider, *European Journal of Mechanics – A/Solids*, **27**(6): 1088–1107, 2008, https://doi.org/10.1016/j.euromechsol.2008.02.005.

15. R.K. Németh, B.B. Geleji, Modal truncation damping in reduced modal analysis of piecewise linear continuum structures, *Mechanics Based Design of Structures and Machines*, **51**(3): 1582–1605, 2021, https://doi.org/10.1080/15397734.2021.1874414.

16. S.W. Shaw, P.J. Holmes, A periodically forced piecewise linear oscillator, *Journal of Sound and Vibration*, **90**(1): 129–155, 1983, https://doi.org/10.1016/0022-460X(83)90407-8.

17. D. Urman, M. Legrand, Nodal-boundary finite-element method for the Signorini problem in two dimensions, [in:] *Proceedings of the ASME 2021 International Design Engineering Technical Conferences & Computers and Information in Engineering Conference*, August 17–20, ASME, Virtual, Online, pp. 1–3, 2021, https://www.researchgate.net/publication/368898096_Nodal-Boundary_Finite-Element_Method_for_the_Signorini_Problem_in_Two_Dimensions.

18. C. Yoong, A. Thorin, M. Legrand, Nonsmooth modal analysis of an elastic bar subject to a unilateral contact constraint, *Nonlinear Dynamics*, **91**: 2453–2476, 2018, https://doi.org/10.1007/s11071-017-4025-9.

Received August 11, 2025; revised version October 22, 2025;
accepted October 27, 2025; published online November 24, 2025.